Experimental Evaluation and Digital Simulation of the UCL Hydraulic Arm Prosthesis

D.R. Broome, B.Sc.(Eng), Ph.D.

Abstract

The UCL hydraulic arm prosthesis, based on the Edinburgh arm linkage, is briefly described, and some of its general performance capabilities outlined. Specific evaluation tests were conducted to assess the dynamic response of the hydraulic servo actuator systems. These included measurements of saturation velocities and stall load capabilities of the main arm articulations. Detailed observations of the shoulder elevation function, the heaviest loaded actuator, were made to provide data on the transient response of this servosystem. A digital computer simulation of this arm function is described. Results of running the digital simulation show a very good correlation with the experimental tests. Some shortcomings of this arm are shown and suggestions made as to how these can be improved, and the paper concludes by reemphasising the considerable advantages to be gained by using hydraulic actuation, illustrated by these test results.

Mech. Eng. Dept., University College London

Introduction

The development of the UCL hydraulic arm prosthesis has been well reported (1), (2), (3), (4), (5). Fig. 1 is a photograph of the arm attached to a harness, with the power pack installed in the body powered arm, and the batteries on a waist belt. The arm is fitted with four servoactuators. The first of these in the forearm section provides wrist rotation giving the terminal device 180° of supination pronation. The compound reach motion is provided by a single actuator sited in the forearm, driving through an elbow block to provide linked motion of shoulder and elbow flexion. Independent shoulder flexion is obtained from the more distal actuator in the upper arm section: humeral rotation is provided by the actuator in the rear of the upper arm. The terminal device, is a modified Otto Bock pneumatic hook which is interchangeable with a cosmetic powered hand. The bowden cables used to operate the valve actuators were each connected to a lever which were all mounted in a lever box unit, so that the arm could be operated in several functions at once by finger movements. The weight of the hydraulically-powered arm, less terminal device, was measured as 1.55 Kg (3.4 lb) which is comparable with the gas powered prosthesis.

Accuracy of positioning the arm tends to be somewhat degraded due to backlash in the arm linkage gearbox, and the effects of the Bowden cable inputs. A quantitative assessment was made by using the arm in a manipulative mode, where it was required to pick up a metal block from a waist high surface and replace it in a defined area on the same surface. Subsequently another block was to be placed on the first and so on. The arm was controlled for this task from the lever box, and after some practise it was possible, though difficult, to co-ordinate the motions of at least two arm functions, so that the task was performed successfully, though neither very smoothly, nor quickly. No comparative tests were made with other prostheses, but improvements in this performance can be expected in clinical application for several reasons. Normally the patient, wearing the harness, has the additional degrees of freedom provided by trunk motions for fine positioning of the arm, and his visual field of view is more directly orientated to the required task. Also, the patient will make control site inputs which result in corresponding arm motions, and being in the position control loop, he will more readily learn co-ordinated movements.

Evaluation of the Arm Dynamics

The arm was rigidly clamped at the shoulder and a series of tests was conducted to assess the saturation velocities of the three main positioning functions of shoulder rotation, elevation and elbow reach. The tests were conducted at a supply pressure of 31 bar (450 psi) and the arm was used without the terminal device fitted. Potentiometers were fitted directly to the arm actuator used, and the resultant motions were recorded from an oscilloscope as the valve input levers were moved as fast as possible over the full range of motion.

The shoulder rotation test was conducted with the elbow straight and the shoulder elevation fully extended, that is, the arm was hanging straight downwards. In this position the shoulder rotation actuator will not have any gravitational loading. The range of motion was 100°, and this was produced in 0.6 s for both abduction and adduction of the arm, as shown in Fig. 2. This represents an average rotational velocity for the system over full range of 3 rad/s.

The elbow reach test was performed with the shoulder fully extended such that the lowered position was a straight arm hanging vertically down, and the raised position was with the elbow flexed to 110°, and hence the shoulder over-extended by 55°. The elbow actuator response was such that an average angular velocity of 2.4 rad/s was obtained as the arm was raised, and this increased to 2.8 rad/s as the arm was lowered at full speed. This discrepancy in angular velocity is obviously associated with the gravitational loads tending to reduce the actuator saturation velocity as the arm is raised, and to increase it as the arm is lowered. For this reason, a more detailed test programme was conducted on the most heavily loaded arm function, that is the shoulder elevation system.

(i) Saturation Velocity Test

The shoulder elevation tests were conducted with the elbow fully extended. The terminal device was not fitted so the load seen by the shoulder elevation actuator is represented by the weight of the arm of mass 1.55 Kg (3.4 lb), acting as its centre of mass at 180 mm (5.2 in) distance from the centre of rotation of the shoulder mechanism. The arm was then raised and lowered at full speed over a range of 120° of motion such that the arm was 30° above the horizontal at the top of its motion. An initial assessment of the arm stall capacity showed that the shoulder elevation actuator was stalled at the horizontal when trying to raise a 0.45 Kg mass positioned at 460 mm (18 in) from the shoulder axis. Four further tests were then carried out with masses of 0.113, 0.225, 0.34 and 0.45 Kg carried in the hand position. The loads of the arm alone, and these four equal increments up to stall are subsequently referred to as loads 1 to 5 respectively. The results of these tests are shown in Figs. 3 (a) to (e) for the five chosen loads, and each trace shows both the arm raising and the arm lowering conditions. The difference in jack saturation velocity rising and lowering is pronounced at each load, though it is difficult to see the variation with load when considering one direction of motion. Table I summarises measurements taken from these traces for just the extreme load limits. The mean saturation velocity with arm rising is thus 22.6 mm/s ± 7.9% which infers an angular velocity of 2.37 rad/s, and this increases to 34.7 mm/s ± 5.5% giving 3.64 rad/s for arm lowering. Thus the average lowering speed is 53.5% greater than the average raising over the full working range of arm loads.

(ii) No Load Transient Test

The arm was held securely down on to a bench and the shoulder axle, which is usually attached to the harness, was positioned so that it over-hung the end of the bench. As the shoulder elevation actuator was operated, the arm remained fixed and just the shoulder stub rotated about the shoulder gearbox, with the passive wrist levelling mechanism being driven as usual. This enabled no-load tests to be conducted, which could not be achieved when raising or lowering the arm, and also prevented undue extra wear or damage resulting from a further series of mechanical tests at saturation velocity of the hydraulic servo. Four transients of the system were recorded, the initial and final transients during extension and flexion. The time constants obtained as the time to move 63% of full valve opening either at the start or at the end of travel were then measured as 25 ms, 28 ms, 24 ms and 26 ms respectively.

A further series of transient tests was conducted with the arm loaded, with masses attached to an extension arm damped to the shoulder stub. The responses recorded at various load conditions are given in Fig. 4 and measure-

ments of the time constants of these transients enable a comparison between the practical results and the theoretical model.

(iii) Stall Load Tests

Stall load tests were performed on the arm to measure the stall forces produced by both the shoulder elevation and elbow reach functions, which are the two heavily loaded arm articulations. The orientation of the arm during testing is shown in Fig. 5 (a) and (b) for the shoulder and elbow tests respectively. It was found that the mass to be added to the end of the arm to stall the shoulder elevation actuator was 0.45 Kg (1 lb) and to stall the elbow system required a mass of 0.9 Kg (2 lb) at the end of the arm. These stall capabilities were considerably below those expected by the design.

Considering the shoulder elevation test, the gearbox output torque to hold the arm horizontal as shown would be 5.09 Nm (45.0 lb in). The theoretical stall force from the actuator of area 303 mm^2 (0.469 in^2) supply pressure is 0.94 KN(211 lbf) and thus a torque of 18.8 Nm (166 lbf in) should be available at input to the shoulder gearbox which has a crank radius of 20 mm (0.787 in). The gearbox ratio is 2:1 to provide the 180° shoulder elevation range from a ±45° crank, and hence the expected output torque should be 9.4 Nm. The loss in torque is thus 4.31 Nm or 46%. The losses are due to actuator stiction and Coulomb friction, inefficiencies in the gearbox and further friction and small load effects due to the wrist levelling mechanism. A similar loss is calculated for the elbow system where for the stalled configuration used, the force required at the actuator can be calculated as 0.32 KN compared with the 0.44 KN which should be available at stall, giving a loss of nearly 30%.

Two simple tests were devised to assess the seal and linkage friction in the shoulder elevation actuator system. A spring balance was attached to the arm at the elbow, and it was used to lift the straight arm, and a reading was taken at the horizontal. This test gave an output torque loss of 0.7 Nm or 7% of the available torque, and this was due to both actuator and linkage Coulomb friction. The second test involved removing the actuator from the arm and measuring the friction effects at the piston rod directly. This gave a stiction force of 30 N falling to a Coulomb force of 18 N as the piston moved, compared with a 0.94 KN stall, resulting in a stiction effect of only 3.2%, but this was considerably more with the pressure on. Thus the major part of the torque losses must be due to gearbox inefficiencies, and a last test was conducted to measure the shoulder elevation gearbox torque efficiency.

(iv) Gearbox Efficiency Test

A high rated spring balance was attached directly to the shoulder gearbox drive link, and as this was loaded up the output arm angle was measured. The input torque can be obtained from a measurement of ϕ, the crank angle:

$$T_{in} = W_{in}\, r \cos \phi$$

The output torque is obtained by measuring θ, the arm angle to give:

$$T_{out} = W \times \sin \theta$$

Thus, the torque effinciency, η, may be calculated from $\eta = 2\, T_{out}/T_{in}$. The results of this test are plotted as the graph of Fig. 6 of η against the

stall ratio γ which is the percentage of actuator stall load applied at input to the gearbox and is defined for each load by $\gamma = W_{in}/940$. This curve shows a sharp fall off in the gearbox torque efficiency with increase in input load, the efficiency having fallen to only 35% for an input force of 50% of the actuator stall force.

Digital Simulation of the Shoulder Elevation System

The development of the programme is summarised in Appendix I. The model incorporates the effects of gravitational load and also includes the saturation non-linearity of the valve flow characteristic.

The first series of runs on the computer model used the same loads as were applied to the arm for the saturation velocity tests above, i.e. loads 1 to 5, and these are defined in Appendix I. The results of the angular displacement against time for both arm rising and falling, and for both the lightest and heaviest load conditions have been plotted as Fig. 7 referred to as Model 1. The characteristics show a sensibly linear increase in angular displacement with time due to the valve flow saturation included in the simulation with smooth transients at start and finish. The general trends are as expected from observations on the arm itself, that is lowering the heaviest load produces the fastest arm motion whereas raising the heaviest is the slowest. The differences in angular velocity are not as large as were measured on the arm itself, and the main reason for this was considered to be the much reduced actual stall capability of the shoulder actuator. The measured output torque at stall was only 5.09 Nm (45 lbf in) as compared with its theoretical value of 9.4 Nm (83 lbf in). Thus we can re-rate the values of the loads 1 to 5, relative to system stall as shown in Table II. It is then possible to calculate the additional mass to be added in the hand position which would produce these actual stall ratios, and use these results in new load conditions for the model which should give equivalent loadings to the arm tests. These new loadings are referred to as loads 6 to 10 and are quoted at the back of Appendix I. The results of running the programme with loads 6 to 10 are drawn as Fig. 8, and this is referred to as Model 2. The variations in saturation velocity are seen to be far greater. The saturation velocity of the jack based on the average velocity for the middle 80% of motion is obtained for Model 2 and given in Table III. The correlation between Model 2 and the actual results is sufficiently good for the model to be used to examine the transient response of the system. Plots of the initial transients for loads 6, 8 and 10 are drawn for both the arm rising and lowering as Figs. 9 and 10 respectively. Both sets of transients show a smooth transition to the saturated flow region. The time constant of the exponential rise to this steady velocity can be measured as the time to reach 63% of full valve opening. The no-load time constant of the system can also be calculated from the standard formula as 23 ms and the variations of stall load ratio γ and loaded time constant T' can be drawn, Fig. 11 curve (a) for the arm rising and Fig. 11 curve (b) for the arm falling.

Discussion

Examination of the saturation velocity test traces, Fig. 3 shows that the transition from rest to full speed and vice versa is smooth with no oscillatory behaviour, and this demonstrates the dynamic stability of the hydraulic servo-system. This behaviour is bourne out by the results of the

computer Model 2 and the comparison between the model and the arm test results can be easily seen from Tables I and III. The model results are within 3% of the experimental results over all the loads considered, and also the variations both between directions and within one direction of motion with load are predicted very well from the model.

A notable feature of the hydraulic servo behaviour under load, which can be seen from these observations, is that even when the load is sufficiently high to cause stall before the end of travel, the saturation velocity of the arm up to stall is only 30% less than the saturation velocity when lowering the same load.

The arm no-load transient tests show an average time constant of 25.8 ms which is only 10% higher than the theoretically-predicted value of 23 ms, and this is due to the slight loading effect of the shoulder axle assembly which is being driven. These no-load results show no significant difference in time constants measured when flexing or extending the shoulder.

The time constant measurements obtained from the results of Fig. 4 are used to draw curve (c) of Fig. 11 which gives the variation of time constant with stall load ratio, γ, for the arm starting with load assisting the motion. The correlation with the theoretically-predicted results from Model 2 is very good and agrees within 10% up to load/stall ratio in excess of 60%. Also, the practical results bear out the theoretically-predicted behaviour that the response is faster at lower arm loadings regardless of the load directionality. The loaded arm gives transient results which show that even though the saturation velocity increased with load for the arm falling, the time constant of the exponential rise still increased as well. That is the lowering arm does eventually fall faster under higher loads, but the transient response is reduced. This is due to a higher inertial load reducing initial acceleration. The loss in transient response is more marked when raising the arm as shown in Fig. 11. The model itself can obviously be used to predict system behaviour to any load, over whatever range of motion, type of input, orientation of system, etc. may be required. Similar models could be used on the other arm functions and a complete multi-fuctional model of the arm developed.

The poor torque efficiency of the gearbox is responsible for a considerable degradation in the performance of this system with respect to its design predictions. At half stall load, which represents the arm alone without terminal device, the efficiency has dropped to 35%, and a major redesign is necessary to improve torque transmission efficiencies.

Conclusions

1. The time constant of the exponential rise of the transients, which increases with added load, was not measured at more than 40 ms, even for the heaviest loads, The requirement that the time constant should be less than 50 ms (6), if deterimental effects or user performance are to be avoided, is thus fulfilled at the worst arm loading. The hydraulic servos exhibited stable non-oscillatory transients under all load conditions. This and the inherant rigidity of a hydraulic system both represent considerable improvements over pneumatic actuation, which oscillates under load.

2. The poor linkage gearbox design was responsible for the drop off in load capability from the design value. For this reason, and also because of the difficulties of arranging a suitable clinical evaluation of this

Edinburgh arm, a current project has involved the development of hydraulic servos for fitting in the B.R.A.D.U. radius vector arm designed by Bottomley (7). This work is complete and a limited clinical evaluation has been undertaken and will be described by Davies (8).

3. The digital simulation developed to describe the behaviour of the shoulder elevation system gives very good correlations with the practical test results. This model could be used to assess the performance of any hydraulic servo driven articulating system.

Acknowledgment

The main development project from which this work is reported recieved financial support from the Department of Health and Social Security.

References

(1) Broome, D.R., Davies, B.L. and Lord, M., 'A total hydraulically powered prosthetic arm system' Eng. in Med., Vol. 3, No. 2, (1974).

(2) Broome, D.R., Davies, B.L. and Lord, M., 'Current experience with a prototype hydraulically powered arm prosthesis' Proc. 5th Conf. Can. Med. & Bio. Eng. Soc., Montreal (1974).

(3) Davies, B.L., 'A prototype portable hydraulic power supply for prosthetic applications' Human Locomotor Engineering I. Mech. E. Brighton (1971).

(4) Broome, D.R., Davies, B.L. and Lord, M., 'A prototype hydraulically powered arm prosthesis' Proc. 5th Int. Symp. on External Control of Human Extremities, ETAN, Dubrovnik, (1975).

(5) Broome, D.R., 'Hydraullic Arm Prosthesis' Ph.D. Thesis, University of London (1976).

(6) McRuer, D.T. and Krendel, E.S., 'Human operator as a servo system element' Jnl of Franklin Inst., Vol. 267, p 511-536 (1959).

(7) Bottomely, A.H., 'An approach to a powered arm with co-ordinate control' Proc. Symp. Basic Problems Pretension, Movement and Control of Artificial Limbs. I. Mech. E. London (1968).

(8) Davies, B.L., 'Clinical Experience of a Hydraulic Powered Arm', Proc. 6th Int. Symp. on Ext. Control of Human Extremities, ETAN, Dubrovnik (1978).

TABLE I Saturation Velocity of Shoulder Elevation Actuator under Load - mm/s

LOAD	RAISING	LOWERING
1	24.4	32.8
5	20.8	36.6

TABLE II Equivalent Arm Loadings

LOAD	OUTPUT TORQUE Nm	$\gamma = \frac{L}{L_S}$ THEORY $\frac{L}{L_S} = 9.4$ Nm	$\gamma = \frac{L}{L_S}$ REAL $\frac{L}{L_S} = 5.09$ Nm
1	2.77	29.5	55.1
2	3.28	34.9	65.1
3	3.79	40.3	75.2
4	4.30	45.8	85.3
5	5.09	53.6	100.0

TABLE III Saturation Velocity from Computer Model 2 - mm/s

LOAD	RAISING	LOWERING
6	25.1	33.5
10	21.3	36.8

APPENDIX I Digital Computer Model of the Hydraulic Arm Shoulder Elevation Actuation System

Equations of Motion

The datum positions are with the jack at midstroke and the arm at 30° below the horizontal.

The simplified flow equation is taken for the valve actuator

$$2Lp + A\dot{x} + \frac{V}{\beta}\dot{p} = Ke\sqrt{2p_s} \qquad (1)$$

An additional condition is added to the normal error equation to include the effect of valve saturation, that is

$$\begin{aligned} e &= y - x \qquad -e_o < e < e_o \\ &= e_o \qquad e_o < e < -e_o \end{aligned} \qquad (2)$$

The hydraulic force produces a torque, $T_1 = Apr$ which is reduced by the gear ratio to give $T_2 = Apr/n$ and this accelerates the arm and balances the steady load effect. Assuming the inertial mass of the piston itself to be negligible, we have

$$\frac{Apr}{n} = I\ddot{\theta}_2 + W\,X\cos(\theta_2 - 30°) \qquad (3)$$

Also, from the arm geometry

$$\theta_2 = n\sin^{-1}\left(\frac{x}{r}\right) \qquad (4)$$

A programme was written in Fortran for execution on the PDP GT44 computer to solve these equations of motion for the shoulder elevation system, for the parameter values defined at the end of this Appendix.

The Programme

Even these reduced equations of motion contain several non-linearities which make the most appropriate solution method a discrete time approximation technique. A simple rectangular approximation was used to

define differentials and using this the following extra equations became necessary to produce a solution:

$$\dot{p}_K = p_{K-1} + T_K \tag{5}$$

$$\dot{\theta}_{2K} = \dot{\theta}_{2K-1} + T\,\ddot{\theta}_{2K} \tag{6}$$

$$\theta_{2K} = \theta_{2K-1} + T\,\dot{\theta}_{2K} \tag{7}$$

The initial conditions for the computation were defined for both the arm rising and arm lowering case so that the solution could be obtained for either. Any other motion of the system could, of course, be examined by re-defining the initial conditions. The programme was written so that the load and solution parameters were interactively defined. The load was defined by the parameters, W, X and I typed in on the keyboard at run time. The solution parameters of iteration step size, T, number of iterations required and number of solution values to print were all entered in the same way before the solution was computed. This enabled the full range of motion or just the initial or final transient to be examined in detail, and also the effect on the accuracy of the solution of the iteration step size would be examined and a suitable value selected for a given computation. The problem solution produces an output of the important system variables of x, θ, p and $\dot{x}$ against time.

Parameters of the Shoulder Elevation System

e_o	= 0.75 mm	(0.030 in)	
β	= $3.4\ 10^5$ KN/m^2	($5\ 10^4$ psi)	
V	= 2.9 ltr/min/mm (KN/m^2)$^{-\frac{1}{2}}$	(1.34 in^3/s lbf$^{-\frac{1}{2}}$)	
P_s	= 31 bar	(450 psi)	
A	= 303 mm^2	(0.469 in^2)	
r	= 20 mm	(0.8 in)	
n	= 2.0		
L	= 475 mm^5 s^{-1} N^{-1}	(210^{-4} in^5 s^{-1} lbf^{-1})	(initially)
	1188 mm^5 s^{-1} N^{-1}	(510^{-4} in^5 s^{-1} lbf^{-1})	(finally)
m	= 0.227 Kg	(0.5 lb)	(nominal)
f_o	= 2.31 Ns/m	(20.4 lbs/in)	
λ_o	= 7.24 KN/m	($6.4\ 10^4$ lb/in)	
M	= 1411 Kg	(8.04 lb s^2/in)	(Load 6)
	3123 Kg	(17.8 lb s^2/in)	(Load 10)

Load	W		X		I	
1	15.20	(3.40)	183	(7.20)	51.8	(0.457)
2	16.28	(3.65)	202	(7.94)	67.5	(0.596)
3	17.39	(3.90)	218	(8.58)	84.4	(0.745)
4	18.51	(4.15)	232	(9.15)	102	(0.900)
5	19.62	(4.40)	257	(10.11)	132	(1.165)
6	18.73	(4.20)	276	(10.87)	146	(1.286)
7	20.78	(4.66)	294	(11.58)	183	(1.619)
8	22.83	(5.12)	309	(12.16)	222	(1.961)
9	24.89	(5.58)	321	(12.64)	262	(2.310)
10	27.96	(6.27)	336	(13.24)	323	(2.847)
	N (lb)		mm (in)		N mm s^2 (lb in s^2)	

FIG.1 HYDRAULIC ARM AND HARNESS

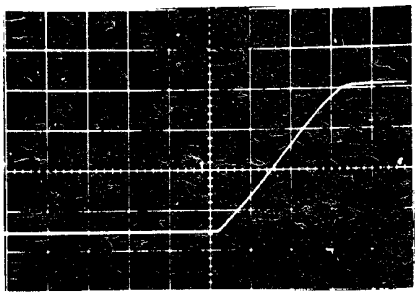

(a) Abduction

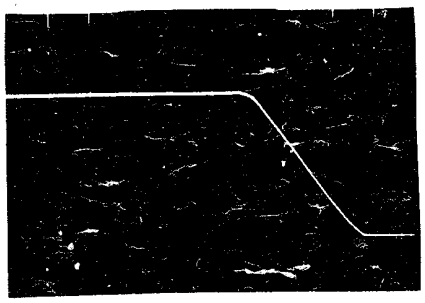

(b) Adduction

FIG. 2 SHOULDER ROTATION RESPONSE

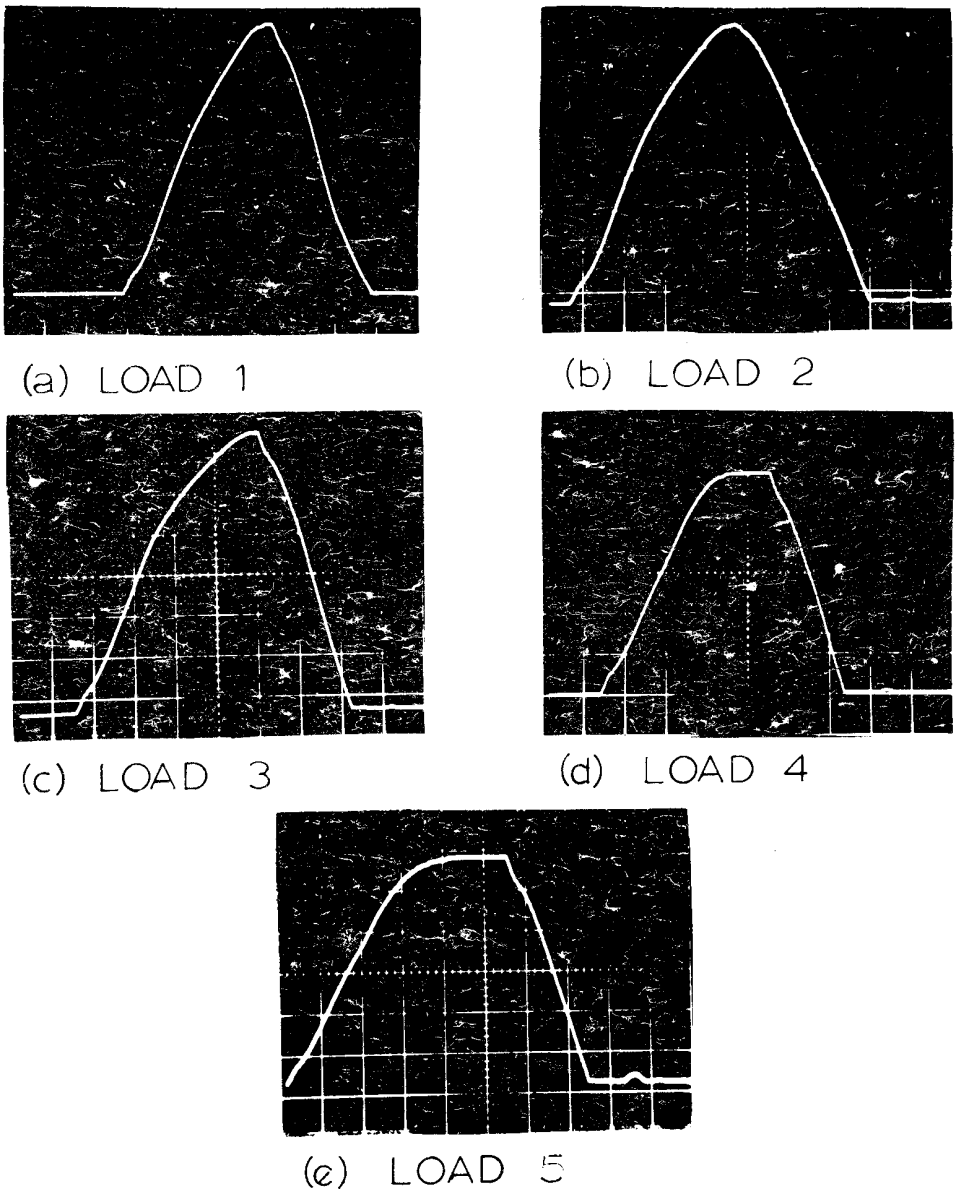

FIG. 3 SHOULDER ELEVATION RESPONSE

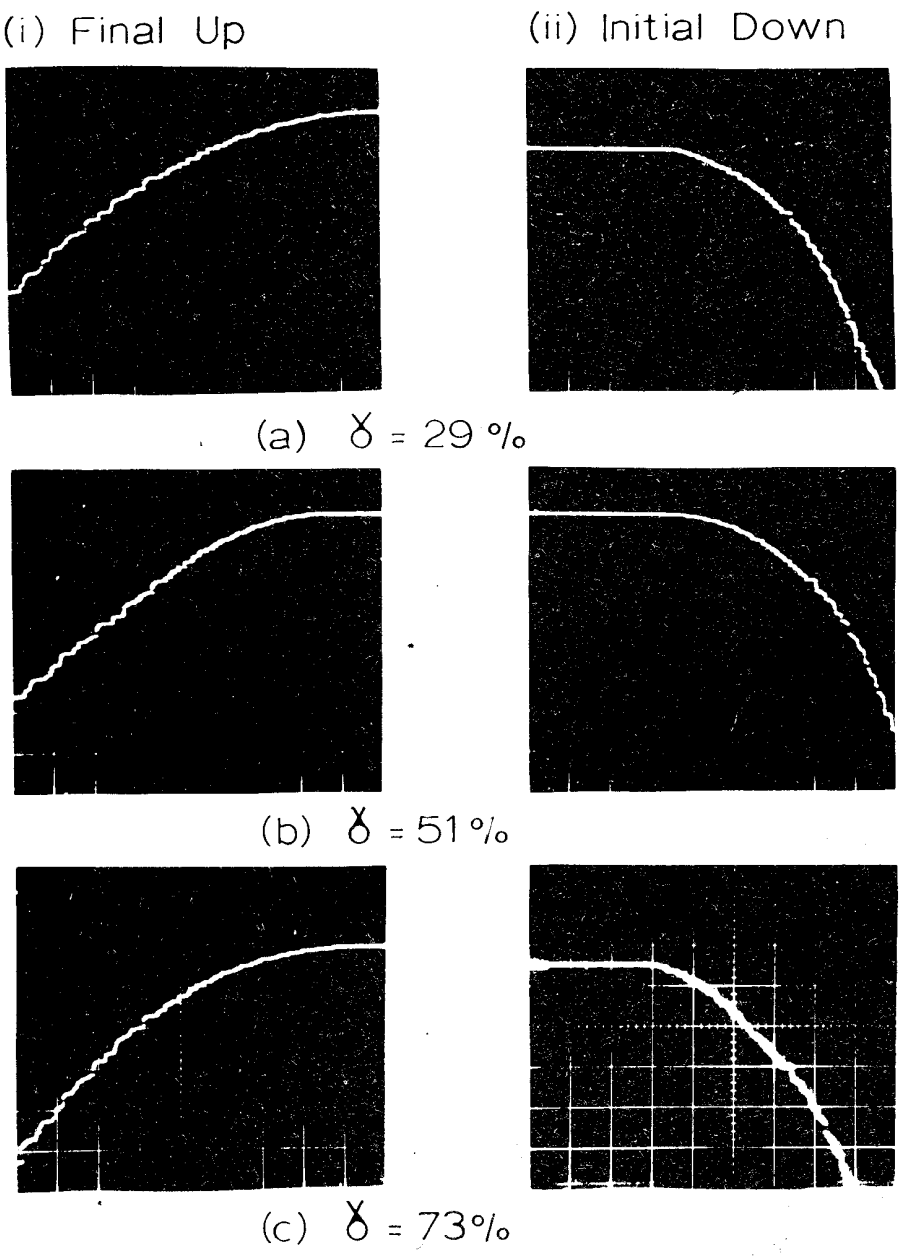

FIG. 4 LOADED TRANSIENTS

SHOULDER ELEVATION

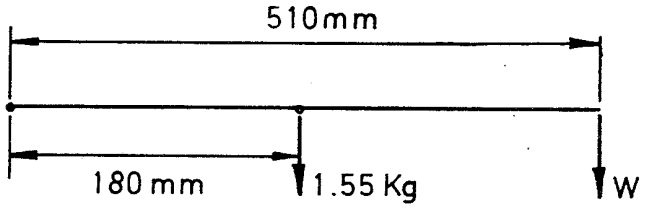

AT STALL W = 4.4N

FIG. 5(a)

ELBOW REACH

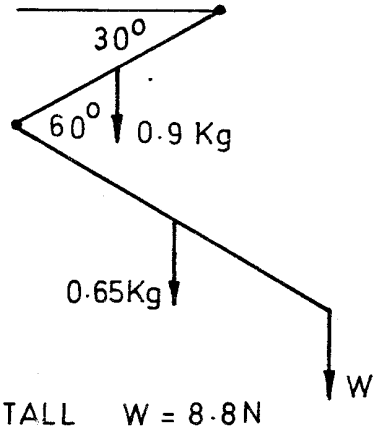

AT STALL W = 8·8N

FIG. 5(b)

ARM ORIENTATION FOR STALL TESTS

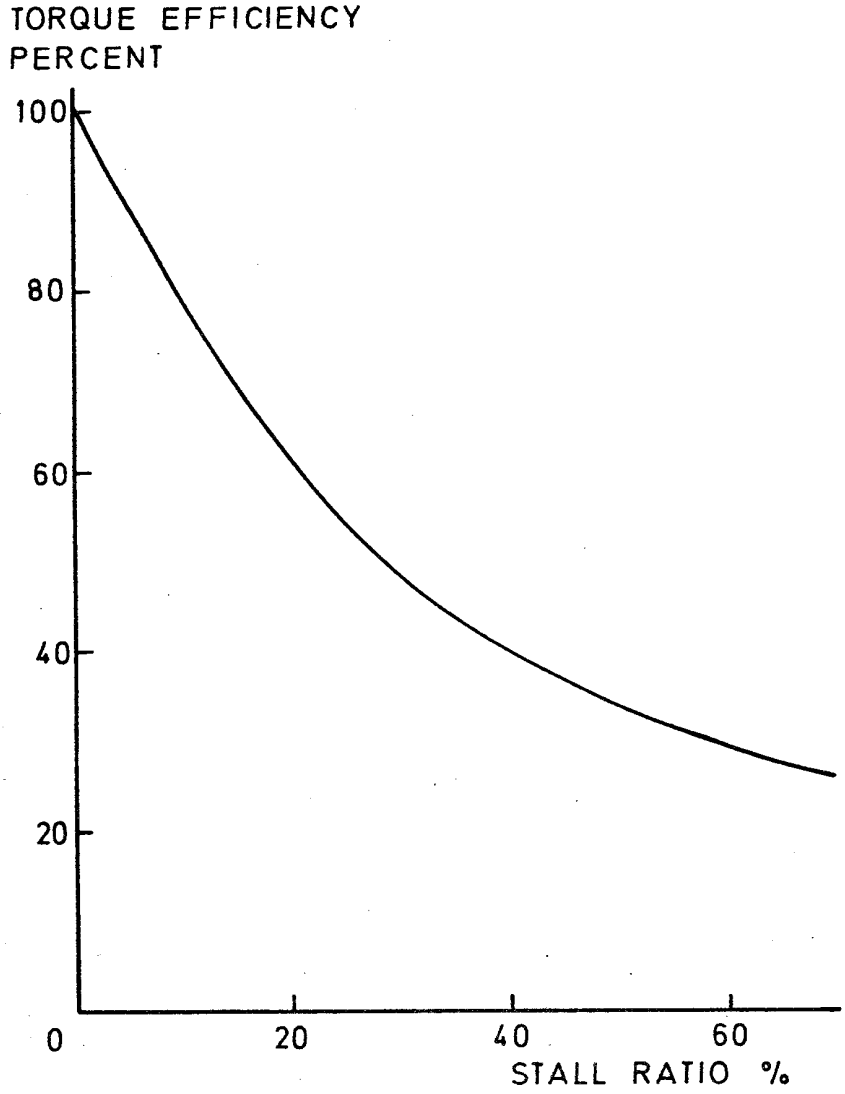

FIG.6 S/E GEARBOX TORQUE EFFICIENCY VS LOAD

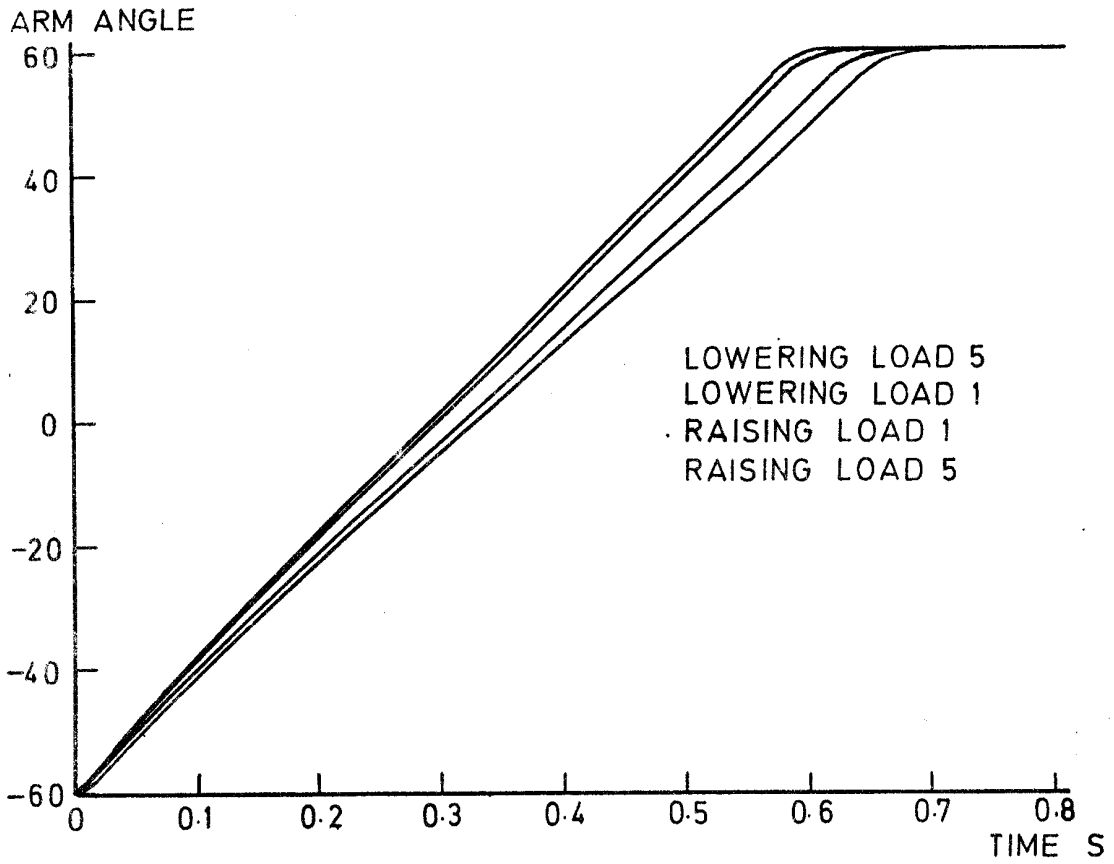

FIG.7 COMPUTER SIMULATION MODEL 1

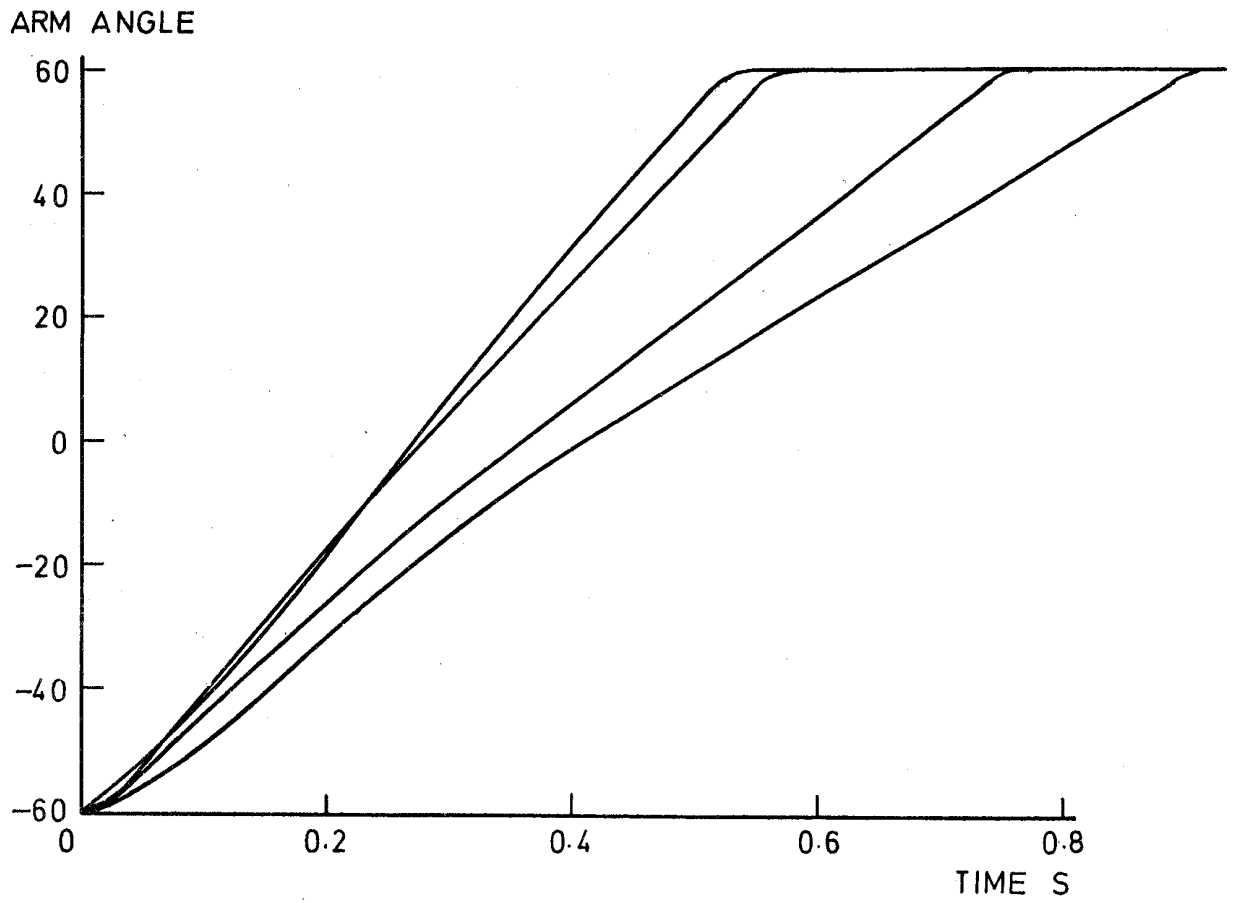

FIG.8 COMPUTER SIMULATION MODEL 2

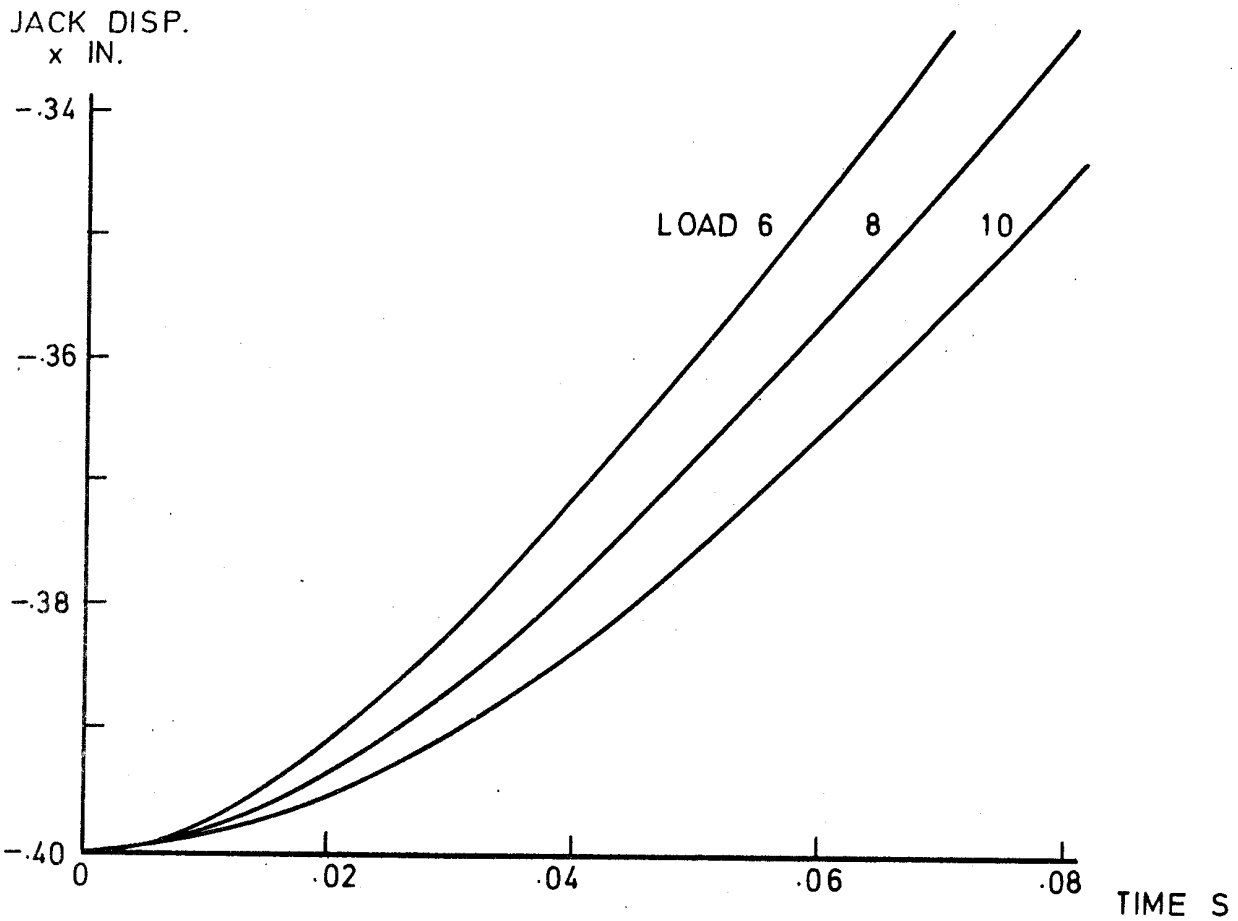

FIG. 9 INITIAL ARM RISING TRANSIENT MODEL 3

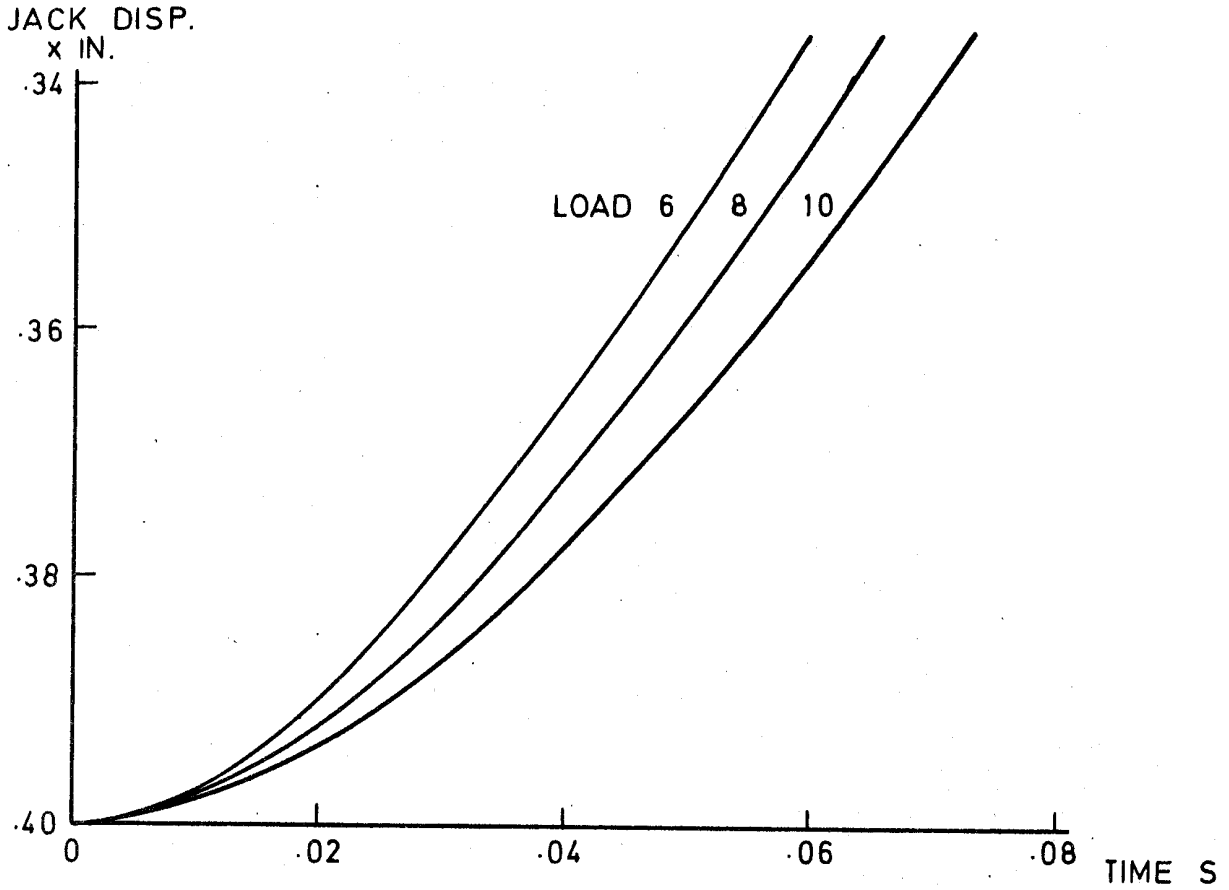

FIG. 10 INITIAL ARM FALLING TRANSIENT MODEL 3

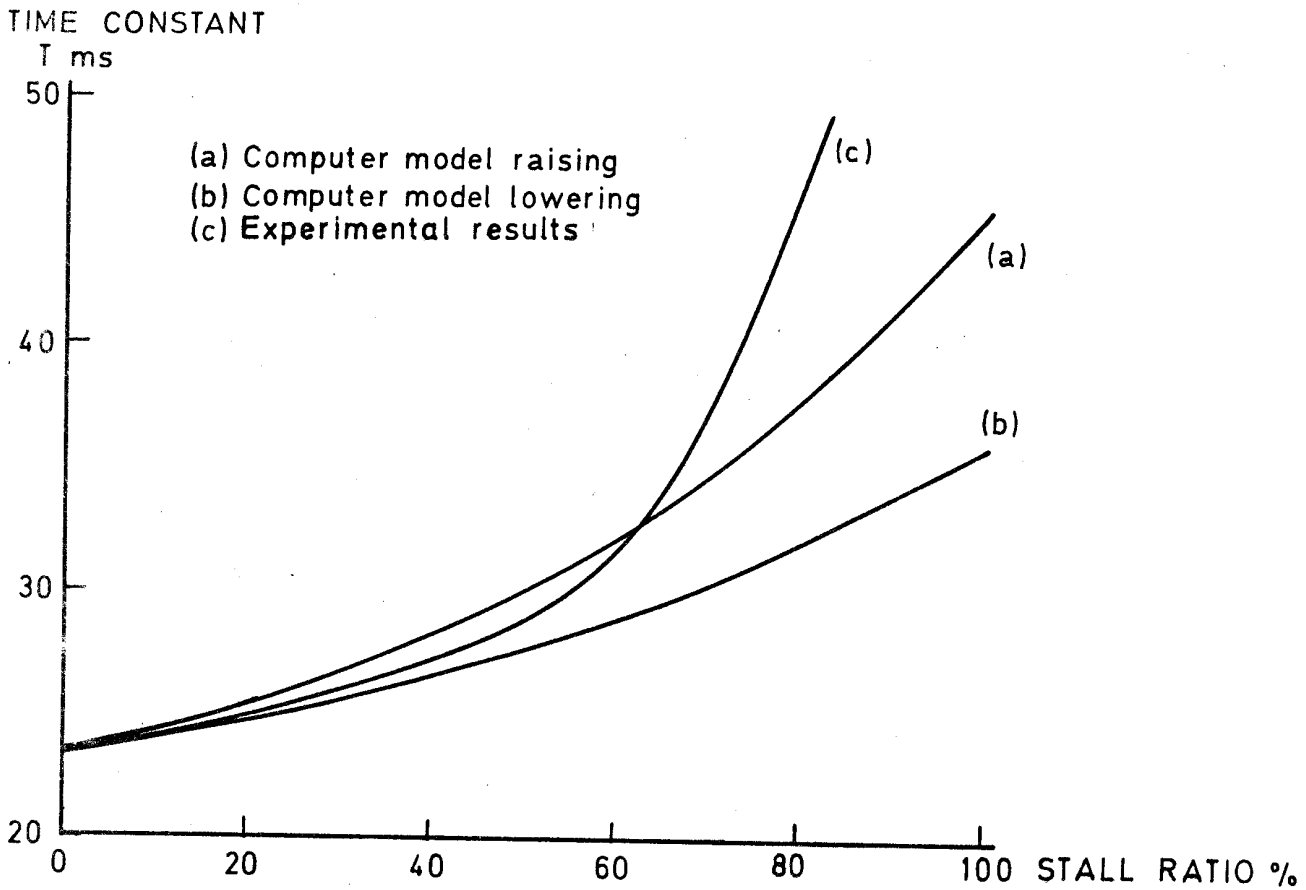

FIG. 11 TIME CONSTANT VS STALL RATIO